Organic Electronics 11 (2010) 881–886

Contents lists available at ScienceDirect

Organic Electronics

journal homepage: www.elsevier.com/locate/orgel

Theoretical maximum quantum efficiency in red phosphorescent organic light-emitting diodes at a low doping concentration using a spirobenzofluorene type triplet host material

Soon Ok Jeon, Kyoung Soo Yook, Chul Woong Joo, Jun Yeob Lee *

Department of Polymer Science and Engineering, Dankook University, Jukjeon-dong, Suji-gu, Yongin-si, Gyeonggi-do 448-701, Republic of Korea

ARTICLE INFO

Article history:
Received 11 September 2009
Received in revised form 28 January 2010
Accepted 2 February 2010
Available online 10 February 2010

Keywords:
Red phosphorescent organic light-emitting diodes
High efficiency
Low doping concentration
Energy transfer

ABSTRACT

Red phosphorescent organic light-emitting diodes (PHOLEDs) with a 100% internal quantum efficiency at a low doping concentration were fabricated using a spirobenzofluorene type phosphine oxide as the host material. A spirobenzofluorene type phosphine oxide compound, 2,7-bis(diphenylphosphoryl)spiro[fluorene-7,11′-benzofluorene] (SPPO21), was synthesized as the electron transport type host material for the red phosphorescent organic light-emitting diodes. The device performances of the SPPO21 based red PHOLEDs were optimized at a low doping concentration of 1–2% because of energy transfer, little concentration quenching and charge trapping. A high external quantum efficiency of 20% was achieved for the red PHOLEDs with the SPPO21 host.

1. Introduction

Phosphorescent organic light-emitting diodes (PHOLEDs) exhibit better quantum efficiencies than fluorescent organic light-emitting diodes and many high quantum efficiency PHOLEDs have been developed. In particular, red PHOLEDs have been widely studied for commercial applications [1].

Typically, organometallic complexes, including Al based organometallic complexes [2], Zn based organometallic complexes [3] and Be based organometallic complexes [4], are used as host materials for red PHOLEDs. Generally, Ir and Pt based organometallic complexes have been applied as red emitting phosphorescent dopant materials [5–8], and the device performances of red PHOLEDs are optimized at a doping concentration between 5% and 20% [6]. The device performance decreases at high doping concentrations because of the concentration quenching effect, whereas the PHOLEDs degrade at low doping concentrations because of an incomplete energy transfer between the host and dopant materials.

However, Kwon's group reported that a high quantum efficiency could be obtained at a low doping concentration of 1% for PHOLEDs with a Be derivative as the host material [4]. The complete energy transfer between the Be type host and the red dopant was responsible for the low optimum doping concentration because of the small bandgap difference of 0.2 eV between the singlet and triplet excitons.

In this work, a spirobenzofluorene type phosphine oxide compound, 2,7-bis(diphenylphosphoryl)spiro[fluorene-7,11′-benzofluorene] (SPPO21), was synthesized as the host material for the red phosphorescent dopant, and the device performances of the red PHOLEDs were investigated. A very low optimum doping concentration of 1–2% and an external quantum efficiency of 20% were observed for the red PHOLEDs with the SPPO21 host. Additionally, the cause of the low optimum doping concentration for the device was elucidated in this work.

---

* Corresponding author. Tel.: +82 31 8005 3585; fax: +82 31 8005 3580.
E-mail address: leej17@dankook.ac.kr (J.Y. Lee).

1566-1199/$ - see front matter © 2010 Elsevier B.V. All rights reserved.
doi:10.1016/j.orgel.2010.02.003

2. Experimental

2.1. Materials

1-Iodo-2-bromobenzene, *n*-butyllithium (n-BuLi), chlorodiphenylphosphine, *N*-bromosuccinimide, naphthalene-1-boronic acid, tetrakis(triphenylphosphine)palladium(0), potassium carbonate, 2,7-dibromo-9-fluorenone were purchased from the Aldrich Chem. Co. and used without further purification. Hydrogen peroxide was obtained from the Duksan Sci. Co. and used without further purification. Tetrahydrofuran (THF) was distilled over sodium and calcium hydride.

2.2. Synthesis

The synthetic route of SPPO21 is shown in Scheme 1. The synthesis of 1-(2-bromophenyl)naphthalene (**1**) and 2,7-dibromospiro[fluorene-7,11′-benzofluorene] (**2**) was described in a previous work [9].

2.3. 2,7-Bis(diphenylphosphino)spiro[fluorene-7,11′-benzofluorene] (**3**)

2,7-Dibromospiro[fluorene-7,11′-benzofluorene] (0.97 g, 1.85 mmol) was dissolved in THF. The solution was cooled to −78 °C and n-BuLi (10 M in hexane, 0.46 mL) was slowly added dropwise. The solution was stirred for 3 h and then a solution of chlorodiphenylphosphine (1.02 g, 4.62 mmol) was added under an argon atmosphere. The resulting mixture was gradually warmed to ambient temperature and quenched with methanol. The mixture was extracted with dichloromethane, and the combined organic layers were dried over magnesium sulfate, filtered and evaporated at a reduced pressure. The white powder that was obtained was purified using column chromatography.

2.4. 2,7-Bis(diphenylphosphoryl)spiro[fluorene-7,11′-benzofluorene] (SPPO21)

A mixture of 2,7-bis(diphenylphosphino)spiro[fluorene-7,11′-benzofluorene] (0.845 g, 1.14 mmol), dichloromethane (10 mL), and 2 mL of 30% hydrogen peroxide was stirred overnight at room temperature. The organic layer was separated and washed with dichloromethane and water. The extract was dried through evaporation to produce a white solid, which was further purified using column chromatography with a final yield of 0.74 g.

SPPO21 yield 83%. T_g 135 °C. ^{1}H NMR (200 MHz, $CDCl_3$): δ 8.75–8.71 (d, 1H), 8.34–7.30 (d, 1H), 7.95–7.84 (m, 3H), 7.70–7.41 (m, 15H), 7.35–7.20 (m, 12H), 7.13–7.06 (d, 2H) 6.73–6.69 (d, 2H). MS (FAB) *m/z* 767 [(M+1)+].

2.5. Characterization

The ^{1}H nuclear magnetic resonance (NMR) was obtained using a Varian 200 (200 MHz) spectrometer. The photoluminescence (PL) spectra were recorded on a fluorescence spectrophotometer (HITACHI, F-7000), and the ultraviolet–visible (UV–vis) spectra were obtained using a UV–vis spectrophotometer (Shimadzu, UV-2501PC). The transition temperature measurements for SPPO21 were carried out using a differential scanning calorimeter (DSC, Mettler DSC 822) at a heating rate of 10 °C/min under a nitrogen atmosphere. The low and high resolution mass spectra were recorded using a JEOL, JMS-AX505WA spectrometer in the FAB (fast atom bombardment) mode. The energy levels were measured using cyclic voltammetry (CV). Atomic force microscopic (AFM) measurements were performed on the evaporated SPPO21 film in order to study the morphological stability of the film.

2.6. Device fabrication

A basic device configuration of indium tin oxide (ITO, 150 nm)/N,N′-diphenyl-N,N′-bis-[4-(phenyl-m-tolyl-amino)-phenyl]-biphenyl-4,4′-diamine (DNTPD, 60 nm)/N, N′-di(1-naphthyl)-N,N′-diphenylbenzidine (NPB, 20 nm)/ 4,4′,4′′-tris(N-carbazolyl)triphenylamine (TCTA, 10 nm)/ SPPO21: iridium(III) bis(2-phenylquinoline) acetylacetonate ($Ir(pq)_2acac$, 30 nm, ×%)/2,9-dimethyl-4,7-diphenyl-1,10-phenanthroline (BCP, 5 nm)/tris(8-hydroxyquinoline) aluminum (Alq_3, 20 nm)/LiF(1 nm)/Al(200 nm) was used for the device fabrication. Various doping

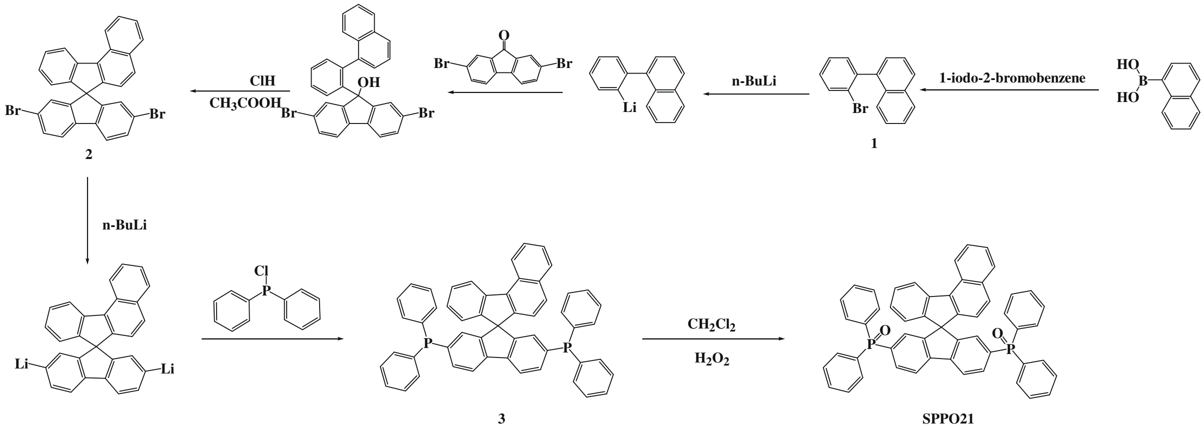

Scheme 1. Synthetic scheme of the SPPO21.

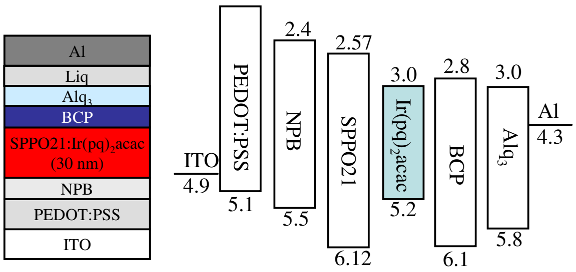

Fig. 1. Device structures of the red PHOLEDs and energy level diagram of the devices.

concentrations of 1% (device I), 2% (device II), 3% (device III), 5% (device IV) and 10% (device V) were used for the red emitting layer. The device structures of the red PHOLEDs are shown in Fig. 1. The photoluminescence (PL) measurements were carried out for Ir(pq)$_2$acac doped SPPO21 using a fluorescence spectrophotometer. Ir(pq)$_2$acac doped solid films with the same doping concentration as the red devices were fabricated for the PL measurements. The current density–voltage–luminance and electroluminescence (EL) characteristics of the red PHOLEDs were measured using a Keithley 2400 source measurement unit and a CS 1000 spectroradiometer. The external quantum efficiency was calculated from the EL spectra, luminance and current density. Lambertian distribution of the light emission was assumed in the calculation of the quantum efficiency and the light emission in the forward direction was measured.

3. Results and discussion

SPPO21 was synthesized through the phosphonation reaction of dibromospirobenzofluorene with chlorodiphenylphosphine. Dibromospirobenzofluorene was effectively prepared through the reaction of dibromofluorenone with 2-bromobiphenyl followed by lithiation and dehydration [9]. The synthetic yield of SPPO21 was 83%, and after purification using column chromatography, the purity of SPPO21 was over 99%. The synthetic scheme of SPPO21 is shown in Scheme 1. SPPO21 was fully characterized using ^{1}H NMR, high performance liquid chromatography, differential scanning calorimetry and high resolution mass spectrometry.

SPPO21, containing a spirobenzofluorene unit and two diphenylphophine units, was used as the electron transporting host material for the red phosphorescent dopant. The spirobenzofluorene moiety has good thermal and morphological stability because of its rigid benzofluorene unit [9]. Additionally, the spirobenzofluorene unit has a triplet bandgap of 2.4 eV, and can be applied as a molecular backbone for the host in red PHOLEDs. The phosphine oxide group isolates the core structure and has electron withdrawing characteristics because of its polarity [10,11]. Therefore, the electron transport properties of the molecule were enhanced by the phosphine oxide group and SPPO21 was an efficient electron transport type host material. Additionally, the energy levels of SPPO21 were effectively managed by the two electron withdrawing phosphine oxide units for efficient electron injection.

Fig. 2 shows the UV–vis and PL spectra of SPPO21. The PL spectra were obtained at both room temperature and 77 K in order to measure the triplet bandgap of SPPO21. SPPO21 exhibited strong absorption peaks at 297 and 340 nm, which corresponded to the absorption of the spirobenzofluorene unit. On the other hand, the diphenylphosphine oxide group did not greatly contribute to the optical absorption. A bandgap of 3.55 eV was calculated for SPPO21 using the absorption edge of the UV–vis spectrum. A PL emission peak was observed at 417 nm because of the wide bandgap of SPPO21. A low temperature PL spectrum was also obtained at 77 K, and the triplet emission peak of SPPO21 was detected at 533 nm with a triplet bandgap of 2.32 eV.

The CV measurements showed that SPPO21 had a HOMO level of 6.12 eV, and a lowest unoccupied molecular orbital (LUMO) of 2.57 eV as well a triplet bandgap of 2.32 eV, which was suitable for transferring energy to red emitting Ir(pq)$_2$acac (triplet bandgap of 2.2 eV). Therefore, SPPO21 can be used as the host in the Ir(pq)$_2$acac doped device.

SPPO21 had a spirobenzofluorene core structure with a twisted fluorene and benzofluorene backbone, which was advantageous for amorphous and thermally stable film formation. Additionally, the diphenylphosphine oxide unit that was connected to the spirobenzofluorene backbone structure also improved the thermal stability because of the polar phosphine oxide group and the phenyl group that was attached to the phosphine oxide unit. Therefore, SPPO21 had a high glass transition temperature of 135 °C.

The surface morphology of the evaporated SPPO21 film was analyzed using AFM in order to study the film stability of SPPO21. The AFM measurements were carried out for a pristine SPPO21 film and an SPPO21 film that was thermally treated at 100 °C for 2 h. The AFM images of SPPO21 are shown in Fig. 3. SPPO21 formed a stable amorphous film with a surface roughness of 0.12 nm. The surface morphology of the SPPO21 film did not change even after thermal treatment at 100 °C for 2 h, and the surface roughness of the SPPO21 film baked at 100 °C was 0.14 nm. Therefore, SPPO21 can effectively be used as a thermally stable host material in organic light-emitting diodes. The stability of the amorphous film was caused by the twisted structure

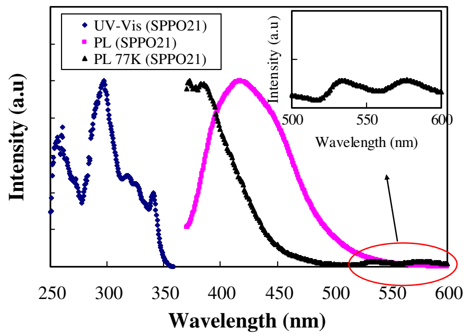

Fig. 2. UV–vis and PL spectra of SPPO21.

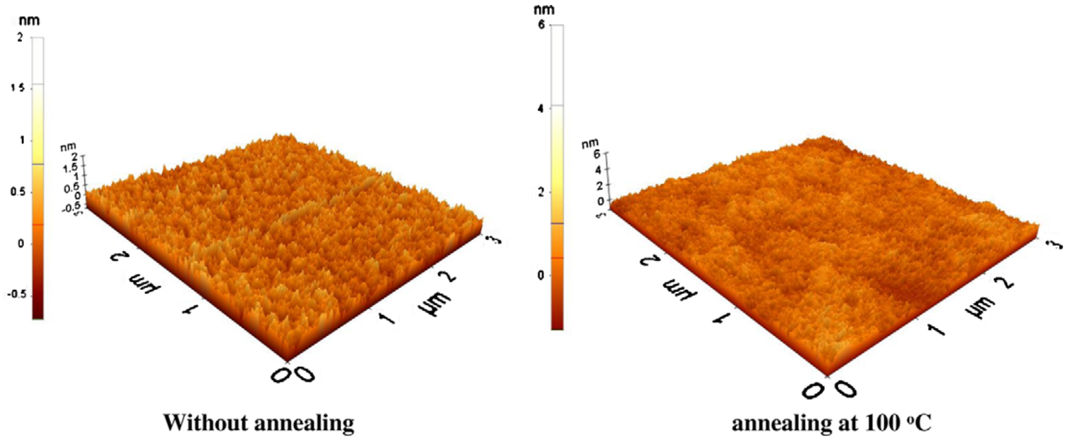

Without annealing annealing at 100 °C

Fig. 3. Atomic force microscopic pictures of the SPPO21 without thermal treatment and after thermal treatment at 100 °C.

of the spirofluorene–benzofluorene core and the two diphenylphosphine oxide units.

The device performances of the red PHOLEDs were studied with respect to the doping concentration of Ir(pq)$_2$acac in order to evaluate the performance of SPPO21 as a host material for red PHOLEDs. Fig. 4 shows the current density–voltage–luminance curves of the red PHOLEDs with different doping concentrations. The current density of the red PHOLEDs increased as the doping concentration increased, and the highest current density was obtained for the red PHOLED with the highest doping concentration. SPPO21 had a HOMO/LUMO level of 6.12/2.57 eV, whereas the HOMO/LUMO of Ir(pq)$_2$acac was 5.2/3.0 eV in the energy level diagram (Fig. 1), corresponding to a HOMO/LUMO level difference of 0.92/0.43 eV between the SPPO21 and Ir(pq)$_2$acac. The large HOMO level gap between SPPO21 and Ir(pq)$_2$acac induced significant hole trapping by the dopant, and electrons were also trapped by the dopant because of the LUMO level gap of 0.43 eV [12]. Therefore, the charge trapping was critical to the current density, and the intermolecular hopping between the dopant materials dominated the charge transport behavior of the SPPO21 device, resulting in high current densities in the highly doped devices.

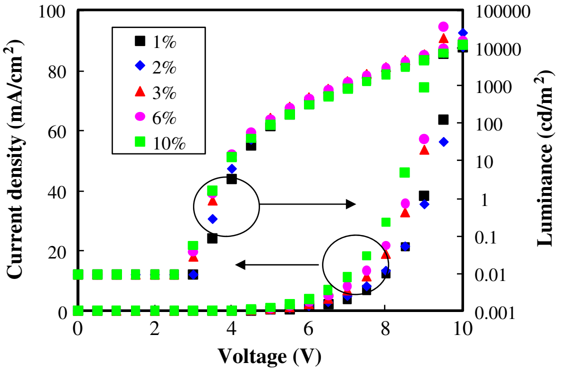

Fig. 4. Current density–voltage–luminance curves of the red PHOLEDs with the SPPO21 host according to the doping concentration of the Ir(pq)$_2$acac.

The luminance of the SPPO21 red PHOLEDs was high at a doping concentration of 3% despite the low current density, indicating a high recombination efficiency in device III. The low luminance of devices I and II was caused by their low current densities. Additionally the luminance of devices IV and V was low because of the low recombination efficiency of the holes and electrons.

Fig. 5 shows the quantum efficiency and current efficiency of the SPPO21 based red PHOLEDs. Device II exhibited the highest quantum efficiency at high luminance (>400 cd/m^2), whereas the quantum efficiency of device I

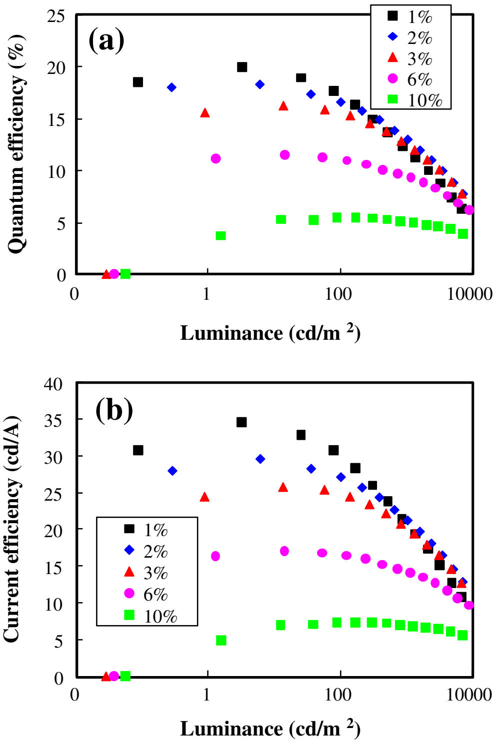

Fig. 5. Quantum efficiency (a) and current efficiency (b) of the red PHOLEDs with the SPPO21 host according to the doping concentration of the Ir(pq)$_2$acac.

was higher than the other devices at low luminance (<400 cd/m^2). The maximum quantum efficiencies of devices I and II were 20% and 18.3%, respectively, whereas the quantum efficiencies at 1000 cd/m^2 were 12.1% and 13.1%, respectively. The quantum efficiency of the SPPO21 device was higher than the SPPO2 that was reported earlier [13]. The external quantum efficiency of device I was the same as the theoretical external maximum quantum efficiency of 20%. However, the quantum efficiency was significantly reduced in devices IV and V. The maximum quantum efficiencies of devices IV and V were only 11.5% and 5.4%, respectively. The quantum efficiency of the SPPO21 based red PHOLEDs was optimized at a very low doping concentration of 1% or 2%. The current efficiency showed the same tendency. However, the reason for this observation was unknown. Therefore, the PL spectra of the Ir(pq)$_2$acac doped SPPO21 films and the EL spectra of the fabricated red PHOLEDs were examined at various doping concentrations.

Fig. 6 shows the PL spectra of the Ir(pq)$_2$acac doped SPPO21 films at different doping concentrations of Ir(pq)$_2$acac. The PL emission of the pure SPPO21 film was observed at around 400 nm with a maximum peak at 405 nm, and the Ir(pq)$_2$acac PL emission was detected at 605 nm. The Ir(pq)$_2$acac doped SPPO21 films exhibited PL peaks for both SPPO21 and Ir(pq)$_2$acac at doping concentrations below 6%, whereas the Ir(pq)$_2$acac doped SPPO21 films exhibited only the Ir(pq)$_2$acac emission at higher doping concentrations above 6%. Therefore, the energy transfer from the SPPO21 host to Ir(pq)$_2$acac was not complete at low doping concentrations. At 6% doping the SPPO21 emission was completely absorbed by Ir(pq)$_2$acac. However, the PL intensity of Ir(pq)$_2$acac was not as strong in the 6% doped SPPO21 film as the others despite the complete energy transfer from SPPO21 to Ir(pq)$_2$acac. The PL intensity of the emitter doped film is affected by the luminescence concentration quenching, which is governed by the doping concentration [14–16]. The concentration quenching rate constant was dependent on R^{-6}, where R is the average distance between dopant molecules. The average distance between Ir(pq)$_2$acac decreased according to the following relationship, $R = [(\text{molecular density in film}) \times (\text{mol\% of the dopant in a film})]^{-1/3}$ [16], and R decreased below 3.0 nm in the 3% doped film. The Förster radius of the phosphorescent emitter doped film was estimated to be below 3 nm [16–18]. Therefore, the concentration quenching was serious above a doping concentration of 3%, resulting in a decrease in the PL intensity. The highest PL intensity was obtained at a doping concentration of 2% because of the small concentration quenching, even though the SPPO21 emission was not completely quenched by the dopant. The low PL intensity at 1% doping was caused by the incomplete energy transfer, whereas the low intensity at 3% doping was caused by the concentration quenching.

The PL intensity of the film was well correlated with the quantum efficiency of the red PHOLEDs. The high efficiency was obtained for device II at a 2% doping concentration, and the efficiency decreased as the doping concentration increased. Even though other factors affected the quantum efficiency of the EL devices, these results proved that the PL emission was critical to the quantum efficiency of the SPPO21 based red PHOLEDs.

Fig. 7 shows the EL spectra of the SPPO21 based red PHOLEDs. The red PHOLEDs exhibited main emission peaks at around 600 nm and the emission peaks were red-shifted at higher doping concentrations because of the intermolecular dipole–dipole interaction that was caused by the short distance between the dopant molecules at high doping concentrations. The main emission peak shifted from 596 nm at 1% doping to 612 nm at 10% doping.

Comparing the PL spectra of the films and the EL spectra of the devices, device I did not show any host emission in the PL spectrum of the 1% doped film. All of the SPPO21 emissions were not absorbed by the 1% doped Ir(pq)$_2$acac in the PL excitation, but the host emission disappeared in the EL emission because of the hole and electron trapping by the Ir(pq)$_2$acac in the energy level diagram of the host and dopant. The excitons were generated not only in the host but also in the dopant because of the charge trapping caused by the large energy level difference between the host and dopant materials. Both the excitons that were formed in the host through the transfer of energy to the dopant and the excitons that were generated in the dopant directly emitted. Therefore, both the energy transfer and the charge trapping were parts of the main mechanism for the light emission in the SPPO21 based red PHOLEDs. The contribution of the charge trapping on the light emission was significant in the highly doped device, but the concentration quenching had a negative effect on the

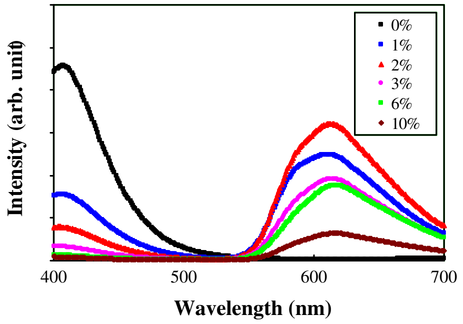

Fig. 6. Photoluminescence spectra of the SPPO21: Ir(pq)$_2$acac film according to the doping concentration of the Ir(pq)$_2$acac.

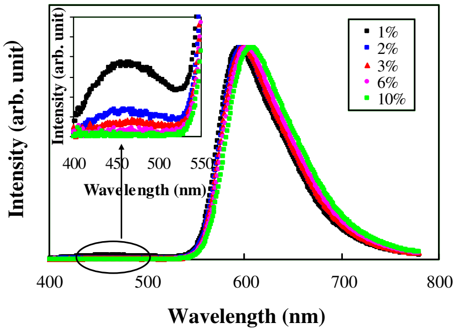

Fig. 7. Electroluminescence spectra of the red OLEDs with the SPPO21 host according to the doping concentration of Ir(pq)$_2$acac.

quantum efficiency. On the other hand, the energy transfer dominated the light emission and the charge trapping compensated for the incomplete energy transfer in the devices with low doping concentrations. Therefore, a high quantum efficiency over 20% was achieved in the SPPO21 based red PHOLEDs.

Even though SPPO21 did not exhibit an emission at 405 nm, a weak emission was detected at 465 nm in the EL spectra of the red PHOLEDs at low doping concentrations. The intensity of the emission weakened at higher doping concentrations and was not observed in device V. An expanded image of the emission peak is shown in Fig. 7 as an inset. This emission peak was caused by the exciplex of TCTA and SPPO21, which was confirmed by the PL emission of the mixed film of TCTA and SPPO21. The electron donating aromatic amine group in TCTA and the strong electron withdrawing phosphine oxide group combined to make the excited complex [19,20]. The TCTA hole transport layer and the SPPO21 host formed the exciplex at the interface, which emitted a weak peak at 465 nm. The exciplex formation was facilitated by the electron accumulation and overflow at the interface between the SPPO21 host and TCTA. Fewer electrons were trapped by the dopant in the red PHOLEDs with lower doping concentrations, leading to better electron transport through the SPPO21 emitting layer. Therefore, more electrons accumulated at the interface and were injected into the TCTA layer in device I, resulting in a relatively strong exciplex emission. The exciplex emission was responsible for the large efficiency roll-off in the red PHOLEDs with low doping concentrations in Fig. 5. A previous report showed that the charge leakage is critical to the efficiency roll-off, and confirming the results that were obtained in this work [21]. The efficiency roll-off decreased as the intensity of the 465 nm peak decreased.

4. Conclusions

The device performances of the red PHOLEDs with the phosphine oxide based SPPO21 host were studied, and a high external quantum efficiency of 20% was achieved. The device performances were optimized at a low doping concentration because of the little concentration quenching, energy transfer and charge trapping. SPPO21 exhibited a high quantum efficiency and low optimum doping concentration making it an effective host material for red PHOLEDs, and therefore, the SPPO21 host material exhibited potential for use in future display and lighting applications.

Acknowledgement

The present research was conducted by the research fund of Dankook University in 2009.

References

[1] J.Y. Lee, J.H. Kwon, H.K. Chung, Org. Electron. 4 (2003) 143.
[2] T. Tsuji, S. Kawami, S. Miyaguchi, T. Naijo, T. Yuki, S. Matsuo, H. Miyazaki, SID Int. Symp. Digest Technol. Pap. 35 (2004) 900.
[3] H. Kanno, K. Ishikawa, Y. Nishio, A. Endo, C. Adachi, K. Shibata, Appl. Phys. Lett. 90 (2007) 123509.
[4] W.S. Jeon, T.J. Park, S.Y. Kim, P. Pode, J. Jang, J.H. Kwon, Org. Electron. 10 (2009) 240.
[5] A. Tsuboyama, H. Iwawaki, M. Furugori, T. Mukaide, J. Kamatani, S. Igawa, T. Moriyama, S. Miura, T. Takiguchi, S. Okada, M. Hoshino, K. Ueno, J. Am. Chem. Soc. 125 (2003) 12971.
[6] M.A. Baldo, M.E. Thompson, S.R. Forrest, Pure Appl. Chem. 71 (1999) 2095.
[7] Y. Kawamura, S. Yanagida, S.R. Forrest, J. Appl. Phys. 92 (2002) 87.
[8] J.Y. Lee, Appl. Phys. Lett. 89 (2006) 223517.
[9] S.O. Jeon, Y.M. Jeon, J.W. Kim, C.W. Lee, M.S. Gong, Org. Electron. 9 (2008) 522.
[10] P.E. Burrows, A.B. Padmaperuma, L.S. Sapochak, P. Djurovich, M.E. Thompson, Appl. Phys. Lett. 88 (2006) 183503.
[11] A.B. Padmaperuma, L.S. Sapochak, P.E. Burrows, Chem. Mater. 18 (2006) 2389.
[12] S. Lamansky, R.C. Kwong, M. Nugent, P.I. Djurovich, M.E. Thompson, Org. Electron. 2 (2001) 53.
[13] S.O. Jeon, K.S. Yook, C.W. Joo, J.Y. Lee, Org. Electron. 10 (2009) 998.
[14] Y. Kawamura, K. Goushi, J. Brooks, J.J. Brown, H. Sasabe, C. Adachi, Appl. Phys. Lett. 86 (2005) 071104.
[15] X. Gong, J.C. Ostrowski, D. Moses, G.C. Bazan, A.J. Heeger, Adv. Funct. Mater. 13 (2003) 439.
[16] Y. Kawamura, J. Brooks, J.J. Brown, H. Sasabe, C. Adachi, Phys. Rev. Lett. 96 (2006) 017404.
[17] I. Tanaka, Y. Tabata, S. Tokito, J. Appl. Phys. 99 (2006) 073501.
[18] G. Ramos-Ortiz, Y. Oki, B. Domercq, B. Kippelen, Phys. Chem. Chem. Phys. 4 (2002) 4109.
[19] S.A. Jenekhe, J.A. Osaheni, Science 265 (1994) 765.
[20] Y. Yang, Q. Pei, Appl. Phys. Lett. 70 (1997) 1926.
[21] S.H. Kim, J. Jang, K.S. Yook, J.Y. Lee, Appl. Phys. Lett. 92 (2008) 023513.